Impaired habit acquisition and striatal dysfunction in early Parkinson's disease

A THESIS
SUBMITTED TO THE FACULTY OF THE
UNIVERSITY OF MINNESOTA
BY

Madhuri Bendale

IN PARTIAL FULFILLMENT OF THE REQUIERMENTS FOR THE
DEGREE OF
MASTER OF SCIENCE

Dr. Steven M. Graves

July 2021

Acknowledgments

First and foremost, I would like to express my deepest gratitude to my advisor, Dr. Steven M. Graves, for giving me the opportunity to work with him and providing invaluable help to this research. His patience, plethora of knowledge, enthusiasm for science, and hard work have deeply inspired me, and it was a great privilege and honor to work under his mentorship.

Besides my advisor, I would like to thank the rest of my thesis committee: Dr. Paul Mermelstein and Dr. Sade Spencer, for their time and consideration.

I thank all my labmates from the Graves Lab: Dr. Yijuan Du, Lauren Boatner, Sanghoon Choi, Alexander Pilski, and Youbin Lee, for their guidance, motivation, and constant support.

Last but not least, I would like to thank my mom, dad, brother, and my best friend Pragya for their firm support throughout my life.

Table of Contents

List of Tables

List of Figures

List of abbreviations

PD - Parkinson's Disease

SNc - Substantia nigra pars compacta

DA - Dopamine

TH- Tyrosine Hydroxylase

L-DOPA - l-Dihydroxyphenylalanine

MPTP- 1-Methyl-4-phenyl-1,2,3,4-tetrahydropyridine

mtDNA- Mitochondrial DNA

SPN- Spiny projection neuron

dSPN- Direct spiny projection neuron

iSPN- Indirect spiny projection neuron

GPi- Internal segment of globus pallidus

SNr- Substantia nigra pars reticulata

GPe- External segment of Globus pallidus

STN - Subthalamic nucleus

LTD -Long term depression

LTP - Long term potentiation

SOR -Spatial object recognition

NOR - Novel object recognition

VTA -Ventral tegmental area

eGFP - Enhanced green fluorescent protein

IHC -Immunohistochemistry

PBS -Phosphate-buffered saline

PFA - Paraformaldehyde

PBS-T - Phosphate-buffered saline with Tween-20

SRS - Systematic random sampling

CE - Coefficient of error

aCSF - Artificial cerebrospinal fluid

2PLSM -Two-photon laser scanning microscopy

CRF- Continuous reinforcement

RI - Random interval

DLS - Dorsolateral striatum

Chapter I: Introduction

1.1 Parkinson's Disease

Parkinson's Disease (PD) is the most common neurodegenerative movement disorder and affects more than ten million people worldwide. Disease etiology remains unknown, with 5-10% of cases having a genetic contribution and the remaining 90-95% of cases being idiopathic (Balestrino and Schapira, 2019). The number one risk factor for PD is age; the occurrence of PD before the age of 50 is rare, but the risk of incidence increases 5-10 fold from the sixth to the ninth decade of life (Poewe et al., 2017; Balestrino and Schapira, 2019). Gender is also a crucial factor in the development of PD. Males are 1.5-2 times more likely to develop PD than females (Baldereschi et al., 2000; Chen et al., 2019). While the cause(s) of PD remains heavily debated and under intensive investigation, it is clear that substantia nigra pars compacta (SNc) dopamine (DA) neurons are among the most vulnerable in PD. In PD, SNc DA neurons progressively degenerate, ultimately leading to the emergence of cardinal motor symptoms such as resting tremor, postural instability, and bradykinesia (Jankovic, 2008).

1.2 Substantia nigra pars compacta and Parkinson's disease

The SNc consists of neurons located within the midbrain that synthesize, package, and release dopamine. These SNc DA neurons primarily project to the striatum (in humans, this brain structure refers to the caudate-putamen), forming the nigrostriatal pathway (Björklund and Dunnett, 2007). Dopaminergic signaling is crucial for various normative behaviors such as voluntary movement, goal-directed behavior, habit formation, motivation, emotion, reward, memory, associative learning, and decision-making (Beninger, 1983; D'ardenne et al., 2012; Pignatelli and Bonci, 2015). Age-dependent progressive loss of SNc DAergic neurons and subsequent DA deficiency is the primary reason for the emergence of motor symptoms, including resting tremor, postural instability, and bradykinesia (Jankovic, 2008). Thus, the production of DA and the integrity of these dopaminergic neurons is of critical importance.

DA is synthesized from the amino acid tyrosine in dopaminergic neurons. Tyrosine hydroxylase (TH), the rate-limiting enzyme in DA production, converts dietary tyrosine to l-dihydroxyphenylalanine (L-DOPA), which, in turn, is converted to DA by the enzyme aromatic amino acid decarboxylase (AADC). After synthesis, vesicular monoamine transporter (VMAT) - 2 transports DA from the cytoplasm into synaptic vesicles. Upon sufficient neuronal depolarization, DA is released into the synaptic cleft for signal

transduction. DA can bind to both presynaptic and postsynaptic DA receptors. Neuronal signaling stops when extracellular DA is removed from the synaptic cleft. In dopaminergic neurons, released DA is taken up from the extracellular space via the dopamine transporter (DAT), where it is either repackaged into vesicles or degraded. Cytosolic DA undergoes oxidative deamination by monoamine oxidase, producing 3,4-dihydroxyphenyl acetaldehyde (DOPAL). DOPAL is further reduced to inactive 3,4-dihydroxyphenyl ethanol (DOPET) or subsequently oxidized to 3,4-dihydroxyphenyl acetic acid (DOPAC) by alcohol dehydrogenase (ADH) or acetaldehyde dehydrogenase (ALDH). (Meiser et al., 2013; Zhang et al., 2019). Dopamine synthesis and metabolism is summarized in figure 1.

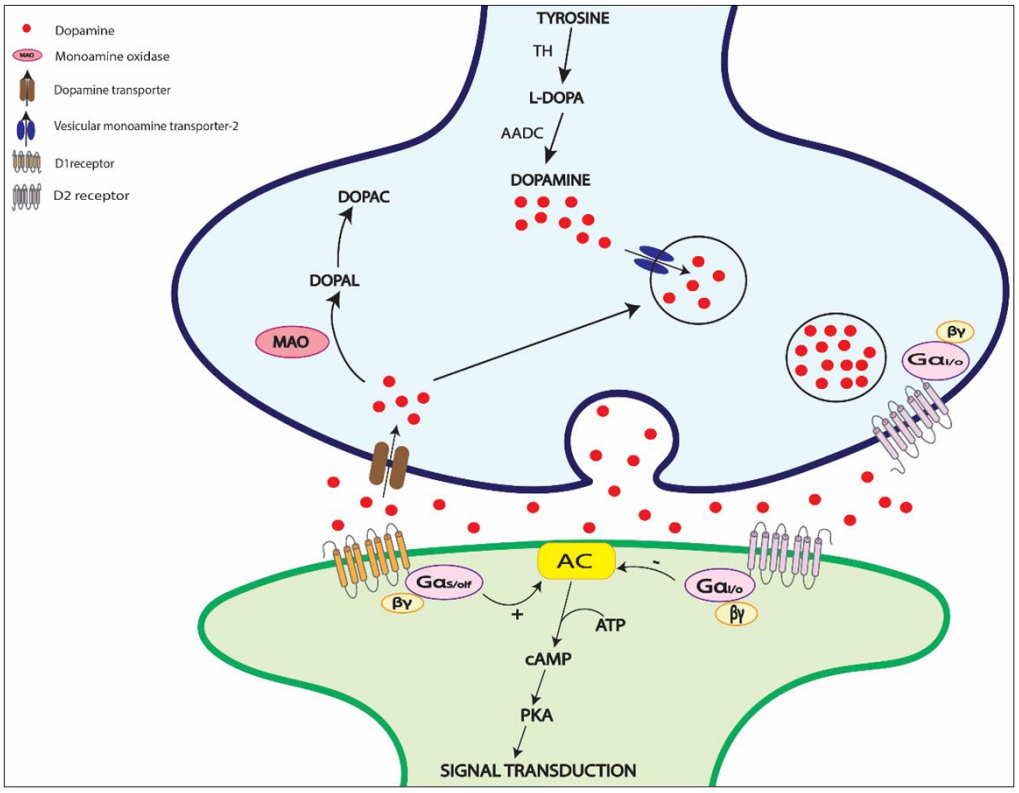

Figure 1: Dopamine synthesis and metabolism. Dopamine is synthesized from tyrosine via sequential reactions catalyzed mainly by TH, and AADC. Dopamine is packaged into synaptic vesicles by VMAT2. Sufficient neuronal depolarization results in synaptic release of dopamine. Synaptic dopamine can bind to both pre- and post-synaptic dopamine receptors. Excessive dopamine is transported back into the neuron by DAT and either recycled or metabolized to inactive metabolite DOPAC by MAO enzyme. Abbreviations: TH, tyrosine hydroxylase; AADC, aromatic amino acid decarboxylase; VMAT2, vesicular monoamine transporter – 2; DAT, dopamine transporter; MAO, monoamine oxidase; DOPAC, 3,4-dihydroxyphenyl acetic acid.

While current therapeutic strategies predominantly focus on DA replacement (i.e., levodopa) or DA receptor agonists (pramipexole), or DA metabolism reduction (selegiline, entacapone), there is currently no disease-modifying therapy (Hegarty et al., 2018; Balestrino and Schapira, 2019). It is most probable that no single mechanism is responsible for PD. Instead, several molecular pathways likely contribute to degeneration, thereby complicating the development of efficacious neuroprotective pharmacotherapy. Mechanisms thought to contribute to SNc degeneration in PD include, but are not limited to, mitochondrial dysfunction, increased cellular stress due to reactive oxygen species, abnormal protein folding and accumulation, microglia-activated neuroinflammation, and loss of trophic factors (Sarkar et al., 2016).

Mitochondrial dysfunction has long been indicated in PD. First, evidence emerged when drug abusers developed parkinsonian symptoms following exposure to 1-methyl-4-phenyl-1,2,3,4-tetrahydropyridine (MPTP). MPTP is metabolized to MPP^+, which inhibits mitochondrial complex-I in dopamine neurons resulting in degeneration (William Langston et al., 1983). Subsequent studies for PD implicated mutations in LLRK2, PARKIN, PINK1, and DJ-1 genes, which encode proteins essential for mitochondrial function, including mitophagy (selective removal of mitochondria), mitochondrial dynamics, and oxidative stress control (Sarkar et al., 2016; Smolders and Van Broeckhoven, 2020). Moreover, SNc DA neurons are hot spots for mitochondrial DNA (mtDNA) deletions. mtDNA deletions cause mitochondrial dysfunction, increased calcium load, and oxidative stress, eventually contributing to neuronal death (Duda et al., 2016; Ricke et al., 2020). Another hallmark feature of PD pathology is the formation of Lewy bodies (LBs), comprising α-synuclein and other proteins. α-synuclein is a presynaptic protein that helps regulate synaptic vesicle transportation and endocytosis. In high concentrations, α-syn converts into pathological oligomers and self-aggregates into higher-order fibrils (Lin et al., 2019). These oligomers and fibrils affect mitochondrial function, ER-Golgi trafficking, protein degradation, and synaptic transmission, inducing neurodegeneration. Mutations in SNCA, LLRK2, PINK1, DJ-1, and PARKIN genes are associated with faulty protein folding, decreased degradation, and increased accumulation of α-synuclein (Lin et al., 2019).

1.3 Striatum and Parkinson's disease

As discussed above, SNc degeneration is paramount to PD; the consequence of SNc degeneration is progressive DA depletion of the striatum, the primary output target of the SNc. The striatum is the largest nucleus of the basal ganglia and is primarily (90-95%)

composed of GABAergic spiny projection neurons (SPNs) (Gerfen and Surmeier, 2011). The remaining 5-10% account for aspiny interneurons, including large cholinergic interneurons. Despite the small number, these interneurons play an integral role in modulating striatal function and associated behaviors. Striatal SPNs are multipolar stellate cells with radially oriented dendrites. These dendrites are covered with small postsynaptic specializations called dendritic spines. Dendritic spines are dynamic and exhibit a variety of morphological characteristics that may be associated with synaptic function. During development and adulthood, SPN dendritic spines may undergo morphological changes, pruning, or increase in number with various treatments and/or disease states (Lanciego et al., 2012; Surmeier et al., 2014; Lynch et al., 2018; Villalba and Smith, 2018). Based on their morphology, spines are categorized into four types: mushroom, thin, stubby, and filipodia. Mushroom spines have a large head and small neck that separates them from the dendrite. Mushroom spines are thought to be mature spines that form strong synaptic connections and are thought to entail circuits responsible for long-term memory storage (Bourne and Harris, 2007). Thin spines are structurally similar to the mushroom spines having a relatively minor head compared to the neck. They are also referred to as learning spines as they are believed to form new memories during synaptic plasticity accompanied by head enlargement (Bourne and Harris, 2007). Stubby spines are relatively shorter and lack a distinct neck. Stubby spines are viewed as immature spines because of their prevalence during early postnatal development and relative scarcity in the mature brain (Harris,' et al., 1992; Berry and Nedivi, 2017). Filipodia are thin, long protrusions of dendritic membrane and are devoid of a clear head. Filipodia are very versatile and flexible structures with a short lifetime and are frequently found in developing neurons (Berry and Nedivi, 2017; Pchitskaya and Bezprozvanny, 2020).

Based on the type of DA receptor expression and projections, SPNs can be categorized into two sub-populations: direct spiny projection neurons (dSPNs) and indirect spiny projection neurons (iSPNs). dSPNs express the D1 DA receptor and directly project to the internal segment of globus pallidus (GPi), and substantia nigra pars reticulata (SNr). D2 DA receptor-expressing iSPNs project to the external segment of globus pallidus (GPe), which further projects to the subthalamic nucleus (STN) (Surmeier et al., 2007). dSPNs gate thalamocortical circuitry by inhibiting GABAergic neurons at basal ganglia interface (SNr) and promotes action selection, leading it to be referred to as go-pathway. iSPNs inhibits GPe, which in turn dis-inhibits the STN resulting in activation of the GABAergic neurons at the basal ganglia interface (SNr and GPi) and suppression of action selection,

leading it to be referred to as no go-pathway (Surmeier et al., 2007). Basal ganglia circuitry is summarized in figure 2.

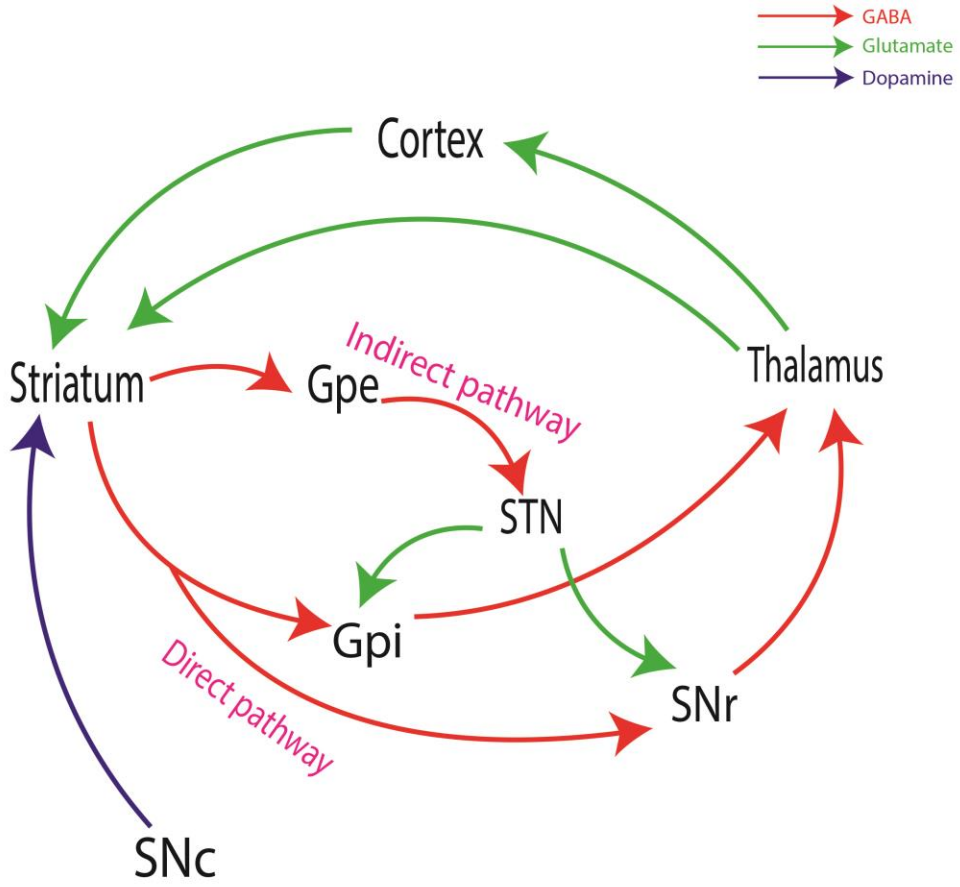

Figure 2: Basal ganglia circuitry. The direct pathway spiny projection neurons project directly to neurons at the basal ganglia interface, namely, neurons of the SNr and GPi. By contrast, indirect pathway spiny projection neurons project axons to the GPe which further projects to STN, which inturn project to the SNr and GPi. Excitatory, glutamatergic inputs to striatal neurons are derived from neurons in the cerebral cortex and thalamus. Red, green and blue arrows represents GABAergic, glutamatergic and dopaminergic projections, respectively. Abbreviations: SNC,substantia nigra pars compacta; SNR, substantia nigra pars reticulata; STN,subthalamic nucleus; Gpi, internal segment of globus pallidus; Gpe, external segment of globus pallidus.

SPNs are the primary targets for striatal extrinsic inputs and receive excitatory glutamatergic inputs from the cortex and thalamus. The thalamostriatal system originates from the thalamus, the caudal intralaminar nuclear complex, comprising the centromedian (CM) and parafascicular (Pf) nuclei in primates is considered as the major source of thalamic afferents to the striatum (Villalba and Smith, 2018). Thalamostriatal circuits account for ~25% of axospinous synapses (Smith et al., 2014). The corticostriatal circuitry

arises from the cortex and accounts for most of the excitatory glutamatergic synapses in the striatum; ~80% of spines on iSPNs and dSPNs form corticostriatal axospinous circuitry (Gerfen, 1988). Additionally, spines receive synaptic inputs from midbrain DAergic neurons, which frequently terminate onto the neck of the spine or a nearby segment of the dendritic shaft, thus providing an anatomical substrate for close synaptic interactions between glutamatergic and dopaminergic inputs (Villalba and Smith, 2018).

DA from SNc inputs has distinct effects on each SPN population based on differential receptor expression and thus regulates neuronal excitability. Both dSPN and iSPNs can undergo forms of cellular learning and memory whereby synapses are weakened (LTD) or strengthened (LTP). In iSPNs, D2 receptor activation engages $G_{i/o}$ protein signaling, decreasing intrinsic excitability and promoting long-term depression (LTD) (Surmeier et al., 2014). In dSPNs, activation of $G_{s/olf}$ coupled D1 receptors increases intrinsic excitability and promotes long-term potentiation (LTP) (Surmeier et al., 2014). Interneurons also help to regulate the neuronal excitability of SPNs. Simulation of D2 receptors on cholinergic interneurons decreases M1 receptor signaling, dis-inhibiting L-type calcium channels allowing LTD in both dSPNs and iSPNs (Augustin et al., 2018). Previous studies indicate that bath application of the A2a receptor agonist in the absence of D2 receptor stimulation promotes induction of LTP in iSPNs (Shen et al., 2008). Thus, both dSPNs and iSPNs are capable of bidirectional synaptic plasticity.

In PD, there is striatal DA depletion causing cell-specific alterations in the intrinsic excitability and synaptic plasticity. The traditional model suggests an imbalance in SPN pathways, with an increased iSPN and decreased dSPN activity thought to contribute to aberrant action selection (Albin et al., 1989). Previous studies also demonstrate that bidirectional plasticity is impaired in SPNs in 6-OHDA lesioned parkinsonian mice (Shen et al., 2008; Thiele et al., 2014). In addition to impairments of synaptic plasticity, striatal SPNs also change spine dynamics. Postmortem analyses of Golgi-stained striatal neurons in PD patients showed significant atrophy of the dendritic tree and loss of spines on SPNs (McNeill et al., 1988). These findings were later replicated in various studies utilizing toxin PD models (Villalba and Smith, 2018). Thus, toxin models of PD demonstrate robust spine pruning and reduced dendritic arborization, as seen in late-stage PD. Whether spine pruning is selective for iSPN or dSPNs is debated. Some studies indicate iSPNs selectivity (Day et al., 2006; Fieblinger et al., 2014b); others demonstrate that both SPNs undergo spine pruning (Escande et al., 2016; Gomez et al., 2019)(Du and Graves, 2019).

1.4 **Non-motor symptoms**

SNc degeneration is primarily associated with motor impairments; consistent with this, restoring DA levels with levodopa therapy improves motor symptoms drastically. However, the cardinal symptoms resultant from SNc degeneration do not occur until >50% of neurons are lost (Fearnley and Lees, 1991; Godau et al., 2012). Thus, years, sometimes decades of SNc degeneration occurs before the onset of the hallmark symptoms. This period is referred to as the pre-motor or prodromal phase of PD (Adler, 2011; Berg et al., 2021). During this period, patients exhibit non-motor symptoms that add to overall disability (Goldman and Postuma, 2014; Weintraub and Mamikonyan, 2019). Fig 3 summarizes the non-motor symptoms seen in PD.

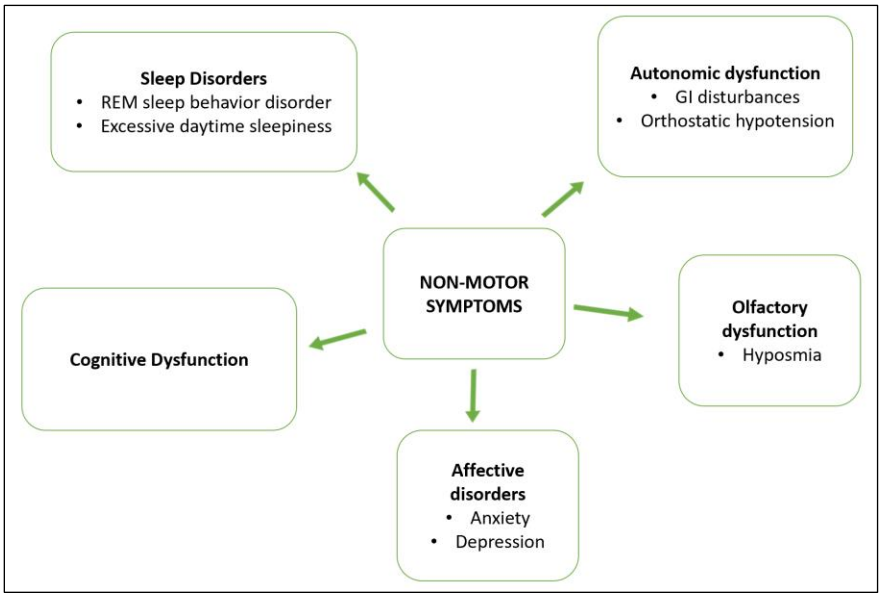

Figure 3: Non-motor symptoms in Parkinson's disease

It is traditionally thought that cognitive dysfunction does not emerge until late in the progression of PD. However, cognitive dysfunction in PD is heterogeneous in its severity, rate of progression, and affected cognitive domains (Goldman et al., 2018). Even though the progression of motor impairment is mainly caused by progressive degeneration of the DAergic nigrostriatal pathway, PD cognitive decline etiology is still unknown. Preclinical studies in animal models of PD also indicate cognitive deficits. A chronic low dose MPTP administration paradigm in non-human primates resulting in a partial lesion produces cognitive deficits in attention and executive function without motor deficits (Schneider, 1990; Decamp and Schneider, 2004). These cognitive deficits are consistent with early behavioral impairments seen in PD patients (Wright MJ, Burns RJ, Geffen GM, 1990;

Maddox et al., 1996; Solari et al., 2013). The 6-OHDA partial lesion model with 40% DA depletion exhibit impaired spatial object recognition (SOR) (Ztaou et al., 2018). Impaired novel object recognition (NOR), SOR, and learning memory deficits are also indicated for the Y-maze test in the transgenic mice model of α-synuclein (Magen et al., 2012). MPTP rodent models show learning memory deficits in a cue-based Morris water maze test (Da Cunha et al., 2006). According to a study conducted by Li et al. in 2013, a PD mouse model with adult-onset progressive SNc degeneration demonstrates deficits during the acquisition phase of the Barnes maze assay and impaired NOR prior to the emergence of motor symptoms.

Although commonly related to motor control disorders, disorders of the basal ganglia have long been known to produce cognitive symptoms (Albin et al., 1989; Shan et al., 2014). The dorsolateral striatum (DLS) part of the basal ganglia circuit is considered the hub of habitual performance. Habits are automated behaviors that are insensitive to changes in behavioral outcomes and are studied in animal models by measuring perseverance of instrumental behaviors (e.g., lever pressing) following changes in reward value or by measuring flexibility in responding during probe trials by manipulating action-outcome contingency (Nadel et al., 2020). Initially, action selection is primarily outcome-dependent, indicating goal-directed behavior. However, with repeated or extensive training, performance shifts from consequence to its antecedents, i.e., the response becomes habitual or stimulus-driven. Lesions to the DLS are associated with impaired habit learning during operant conditioning procedures in rodent models (Yin et al., 2004; Faure et al., 2005; Yu et al., 2009; Shan et al., 2014; Nadel et al., 2020). Before the appearance of motor symptoms, more than 80 percent of the striatum is depleted of DA (Godau et al., 2012). Very little is known about the changes occurring in the striatum and the behavioral consequences of that in PD. Thus, evaluation of habit acquisition during pre-motor PD could potentially serve as a valuable tool for developing a behavioral biomarker for early diagnosis of PD.

1.5 Animal models in Parkinson's disease

Two main approaches are commonly used to study PD in experimental animals, namely toxins and genetic models. Toxin models are generated by injecting neurotoxins (6-OHDA & MPTP), herbicides/pesticides (rotenone & paraquat), or ubiquitin-proteasome system (UPS) inhibitors (Duty and Jenner, 2011; Le et al., 2014; Kin et al., 2019), resulting in rapid and overt SNc degeneration. UPS inhibition models can also generate intracellular α-

synuclein accumulation (Xie et al., 2010). However, toxin models are acute in nature in that they produce a rapid cell loss in the SNc and, unless carefully titrated, produce a robust lesion emulating late-stage PD and lack the progressive nature of the disease. Although most PD incidences are sporadic, around 5-10% of PD cases have genetic linkage (Balestrino and Schapira, 2019). Multiple genes have been implicated in PD, including SNCA, LRRK2, PRKN, PINK1, and PARK7 (Balestrino and Schapira, 2019). More recent models employ genetic manipulations that either introduce these familial mutations or selectively disrupt nigrostriatal neurons (Pitx3, Nurr1) (Wager, 2011; Stoker and Greenland, 2018; Kin et al., 2019). While these models can recapitulate specific PD aspects, they fail to demonstrate neuronal degeneration associated with PD. Even the aged parkin/DJ-1/PINK1 triple knockout model fails to show nigral degeneration (Kitada et al., 2009). Pitx3 -/- animals demonstrate selective loss of DAergic neurons, but in this model, most neurons fail to develop and do not innervate the striatum fully. Thus it is a model with neurodevelopmental deficits rather than a parkinsonian model of degeneration.

The mitopark mouse model, however, produces adult-onset progressive SNc degeneration. The mitopark mouse lacks mitochondrial transcription factor A (Tfam), specifically dopaminergic neurons (Galter et al., 2010). Tfam is necessary for mitochondrial transcription and is also required for mtDNA maintenance in mammals; it stabilizes mitochondrial DNA, regulates mtDNA copy number in-vivo, and is essential for mitochondrial biogenesis (Larsson et al., 1998). Neurons lacking Tfam develop progressive respiratory chain deficiency followed by cell death (Larsson et al., 1998). Mitopark mice faithfully recapitulate key parkinsonian features (Ekstrand et al., 2007). These include progressive, selective loss of SNc DA neurons over that of the ventral tegmental area (VTA), spontaneous vertical and horizontal locomotor deficits that improve with L-DOPA treatment, cognitive dysfunction preceding motor impairments, and decreased striatal DA (Galter et al., 2010; Good et al., 2011; Li et al., 2013; Branch et al., 2016). They also reproduce the sex difference and GI disturbances associated with PD (Chen et al., 2019; Ghaisas et al., 2019).

Since the mitopark mice model can closely mimic the progressive neurodegeneration seen in humans, it serves as a valuable tool to study various aspects of non-motor dysfunction in PD. One such aspect would be to study how changes in the striatum during early PD impact habit acquisition.

Chapter II: Methods

2.1 Animals

Gender is a crucial factor in the development of PD. Males are at higher (1.5-2 times) risk than females for developing PD (Baldereschi et al., 2000). According to a study conducted by Chen et al., there is delayed DA dysfunction and motor deficits in female mitopark mice. Hence, only male mice were used for studies.

A Cre/loxP recombination strategy was used to generate mitopark mice. Briefly, mitopark mice were bred on a C57BL/6J background in which the DA transporter (DAT) promoter was used to drive recombinase Cre expression, and these mice were crossed with mice containing a loxP-flanked Tfam gene (Ekstrand et al., 2007). The mitopark mice used in the experiments were heterozygous for DAT-cre expression and homozygous for the loxP flanked Tfam gene. Mice homozygous for loxP flanked Tfam gene, and negative DAT-Cre expression was used as Tfam control. Enhanced green fluorescent protein (eGFP) was expressed in Tfam and mitopark mice under the control of *Drd2* receptor regulatory elements to produce D2-Tfam and D2-Mitopark mice, respectively. These mice were hemizygous for eGFP expression. tdTomato was expressed under the control of *Drd1a* receptor regulatory elements in Tfam and Mitopark mice to produce D1-Tfam and D1-MitoPark mice, respectively. These mice were hemizygous for tdTomato expression.

Mice were group-housed with water and food provided ad libitum and were maintained in a 12hr/12hr light/dark cycle at controlled humidity and temperature. Subjects that underwent operant procedures were singly housed and food-restricted as described in section 2.6.1. Experiments were reviewed and approved by the University of Minnesota Institutional Animal Care and Use Committee.

2.2 Immunohistochemistry

8 and 12-week old Tfam and mitopark (DAT-Cre-Tfam) mice were used. Animals were anesthetized with an intraperitoneal injection of ketamine (50 mg/kg)/xylazine (4.5 mg/kg) and transcardially perfused using phosphate-buffered saline (PBS) and 4% paraformaldehyde (PFA). Brains were fixed at 4^{o}C overnight using 4% PFA. Brains were sunk in cryoprotecting 30% sucrose solution. Brains were sliced coronally into 40 µm thick slices using a microtome (SM2010R, Leica Microsystems) and stored in PBS.

Twelve slices were selected at an interval of three. Firstly antigens were retrieved by incubating slices in 20% formic acid solution in phosphate-buffered saline with Tween-20 (PBST) solution for 20 mins. Slices were given washing with PBST. 3% Triton-X-100, 5% Donkey serum in PBST was used as blocking solution. Slices were incubated for 30 mins in blocking solutions. Slices were washed with PBS-T and additionally blocked with donkey anti-mouse IgG (1:200) in PBST for 30 mins. After washing with PBS-T, slices were incubated overnight at 4^{o}C in polyclonal rabbit anti-TH antibody (AB152 Millipore, 1:2000) diluted in serum blocking (1:4) solution. The next day, slices were washed with PBST and incubated for 1.5 hours at room temperature in Alexa fluor-555 conjugated antibodies (A31572 Invitrogen, anti-rabbit IgG; 1:200) diluted in serum blocking (1:8) solution. Slices were mounted using Thermo Fisher Scientific Prolong Diamond Antifade Mountant. Slices were allowed to dry overnight before cells were serologically quantified.

All brains were harvested and sliced by Lauren Boatner. Brains were stained and mounted by Lauren Boatner and Madhuri Bendale.

2.3 Stereology

Stereological quantification was done using a Zeiss Axio Imager 2 (Carl Zeiss) attached to a motorized stage and connected to a computer running the StereoInvestigator software (version 2020.2.2, MicroBrighfield Inc). Stereology is the spatial interpretation of two-dimensional cross-sections of tissues using systematic random sampling (SRS). An optical fractionator probe was used to estimate the number of TH^{+} cells. SRS was used with the optical fractionator probe (Gülsüm Deniz et al., 2018) to obtain a set of unbiased virtual counting spaces covering the entire region of interest. Counting sites were sampled by the software at a constant interval to encompass the entire region and avoid any bias. A cube or 3D rectangle represents the sampling site within the region of interest where cells are counted. A disector in 2D is the counting frame where cells were counted. Guard zones are set at the top and bottom to avoid cells damaged by tissue shrinkage.

SNc boundaries were delineated under 2.5x/0.085 NA objective lens. Cell counting was performed on 11-12 slices under a 63x/1.4 NA lens using a counting frame of 150 µm X 150 µm, a grid size of 250 µm X 275 µm, and a 3 µm top and bottom guard zones. The above-described parameters are summarized in Table 1. Tissue thickness was measured at each sampling site for a more accurate estimation. Stereological parameters used resulted in a Gundersen coefficient of error (m=1) (Gundersen et al., 1999), a metric estimating counting precision, of 0.03-0.05.

Data was collected and analyzed by Madhuri Bendale.

Table 1: Stereology summary

Sections	
Number of sections	10--12
Section cut thickness	40 µm
Sampled thickness (mean ± s.e.m.)	32.5± 0.7 µm
Sampling	every 3rd section
Optical fractionator probe	
Counting frame	150 µm X 150 µm
Grid size	250 µm X 275 µm
Dissector height	15 - 25 µm
Guard zone (top and bottom)	3µm
Coefficient of error	
Gunderson (m=1)	0.03 - 0.05

2.4 *Ex-vivo* brain slice preparation

8 and 12-week old D1-Tfam, D2-Tfam, D1-Mitopark, and D2-Mitopark mice were anesthetized with an intraperitoneal injection of ketamine (50 mg/kg)/xylazine (4.5 mg/kg) and transcardially perfused with an ice-cold low Ca^{2+} artificial cerebrospinal fluid (aCSF) containing in mM: 124.0 NaCl, 3.0 KCl, 1.0 CaCl2, 2.0 MgCl2, 26 NaHCO3, 1.0 NaH2PO4, and 16.66 glucose. Once mice were perfused, the brain was rapidly removed, and 275 µm thick sagittal slices containing the dorsolateral striatum were obtained using a vibratome (VT1200S, Leica Microsystems). Slices were transferred to a holding chamber containing normal aCSF with 124.0 mM NaCl, 3.0 mM KCl, 2.0 mM CaCl2, 1.0 mM MgCl2, 26 mM NaHCO3, 1.0 mM NaH2PO4 and 16.66 mM glucose and allowed to recover for at least 30–40 min before experiments. All solutions were pH 7.4 and 300–310 mOsm and were continually bubbled with carbogen (5% CO_2; 95% O_2).

Dr. Steven M. Graves and Sanghoon Choi prepared *ex-vivo* brain slices.

2.5 Electrophysiology and Two-photon laser scanning microscopy

2.5.1 Spiny projection neurons intrinsic excitability

iSPNs and dSPNs in the dorsolateral striatum were identified by somatic eGFP (490–560 nm) and tdTomato (554–581 nm) using a LED, respectively. SPNs were patched in whole-cell configuration using an Ultima Laser Scanning Microscope system (Bruker) with a Nikon FN-1 microscope, a 60X/1.00 NA lens, and PrairieView software. Patch pipettes were pulled from thick-walled borosilicate glass on a Sutter P-1000 puller and filled with a

recording solution. Pipette resistance was typically 3–4.5MO when filled with recording solution. Recording solution contained 135.0 mM KMeSO4, 5.0 mM KCL, 10.0 mM HEPES, 2.0 mM Mg-ATP, 0.5 mM Na-GTP, 5 mM phosphocreatine-Tris, 5.0 mM phosphocreatine-Na, 0.1 mM spermine; pH was adjusted to 7.25–7.30 and osmolarity 270–280 mOsm. Alexa 568 (50 μM) and Fluo-4 (200 μM) dyes were included in recording pipettes. Slices were continuously perfused with carbogen (95% O2; 5% CO2)-bubbled aCSF and maintained at 32–34°C. Whole-cell patch-clamp recordings were obtained using a multi-clamp 700-B amplifier. Intrinsic excitability was assessed in the current clamp with 500ms somatic current injections (20 pA steps) (Fieblinger et al., 2014a; Graves and Surmeier, 2019).

Experiments were performed by Dr. Steven M. Graves and Sanghoon Choi. Madhuri Bendale analyzed data for intrinsic excitability.

2.5.2 Two-photon laser scanning microscopy

After electrophysiology, two-photon laser scanning microscopy (2PLSM) was used to obtain images of the dendritic segment. Alexa 568 (50 μM) dye was included in recording pipettes for imaging. High-magnification images of dendritic segments (proximal: < 80 μm from soma; distal: >80 μm from the soma) were acquired using 810 nm excitation with 0.15 μm x 0.15 μm pixels with 0.3 μm z-steps (Fieblinger et al., 2014b; Graves and Surmeier, 2019). High magnification images were deconvolved using ImageJ software, and semi-automated spine counting was performed using Neurolucida360 (MBF Bioscience).

Experiments were performed by Dr. Steven M. Graves and Sanghoon Choi. Dr.Yijuan Du analyzed the data for spine anatomy.

2.6 Operant behavior

2.6.1 Food restriction and operant chambers

Tfam, Mitopark, D1-Mitopark, and D2-Mitopark mice were used. 7-10 days prior to training, all mice were individually housed and placed on a food deprivation schedule to reduce their weight to 80-85% of their free-feeding weight. All mice were 8-weeks old when they began operant training. After the training has been initiated, mice were fed 1.5-2.5g standard chow each day after the training based on the number of pellets earned. Water was available at all times (Yu et al., 2009).

Training and testing took place in modified Med Associates operant chambers housed within light-resistant and sound-attenuating walls. Each chamber was equipped with a food magazine that received Bio-Serv 14 mg pellets from a dispenser. Each chamber contained two retractable levers (active and inactive) on either side of the magazine and a house light mounted on the same wall side as that of the levers and magazine. A computer with the Med-PC-IV program was used to control the equipment and record behavior.

2.6.2 Lever press training

At the beginning of each session, the house light was turned on, and levers were inserted. At the end of each session, the house light was turned off, and the levers were retracted. Mice were trained on a continuous reinforcement (CRF) schedule (i.e., each active lever press was rewarded with a pellet) for four days. Each session ended after 90 min or 30 rewards, whichever came first. After CRF training, mice were trained on a random interval (RI) schedule to generate habitual lever pressing. First, mice were trained for two days on 30s RI (rewards received on an average of 30 seconds contingent upon active lever press). For the next three days, mice were trained on 60s RI (rewards received on an average of 60 seconds contingent upon active lever press) (Dickinson et al., 1983; Yu et al., 2009).

Figure 4: Habit acquisition timeline

2.6.3 Outcome devaluation

A satiety procedure was used for outcome devaluation (Yu et al., 2009). This procedure controls the overall level of satiety and motivational state while altering the current value of a specific reward. Mice were given unlimited access for one hour to either home chow (non-devalued) or high purified pellet (devalued). The home chow served as a control for the overall level of satiety. After one hour of unlimited access, the mice were subjected to a brief 5 min probe test, during which levers were inserted, but no pellet was dispensed. This brief extinction test is designed to test whether the acquired lever pressing of the mice was controlled by the action-outcome instrumental contingency or elicited by

antecedent stimuli. On the second day of outcome devaluation, the same procedure was used, except that those animals that received home chow on day 1 receive purified pellets on day 2, and vice versa.

Madhuri Bendale wrote the operant program and performed behavioral experiments.

2.7 Statistical analyses

Prism (GraphPad Software La Jolla, CA) was used for all statistical analyses. Data are presented as box-and-whisker plots illustrating the median, quartiles, and range; data from devaluation tests are similarly presented as box-and-whisker plots with the addition of individual data points overlaid. Non-parametric Mann-Whitney (two-tailed) and Kruskal-Wallis with Dunns *post-hoc* analyses were used to determine significance with $\alpha=0.05$.

Chapter III: Results

3.1 Substantia nigra pars compacta dopamine neurodegeneration

The earliest time point reported in the literature demonstrating SNc degeneration is 12 weeks (Ricke et al., 2020); however, striatal DA deficits have been reported as early as eight weeks (Chen et al., 2019). Tfam and mitopark mice were aged for 8 and 12 weeks of age to stereologically quantify the number of TH^+ cells in the SNc. At eight weeks of age, there was no SNc degeneration (Fig. 5A), but at 12 weeks of age, there was ~25% loss of SNc TH^+ cells (Fig.5B).

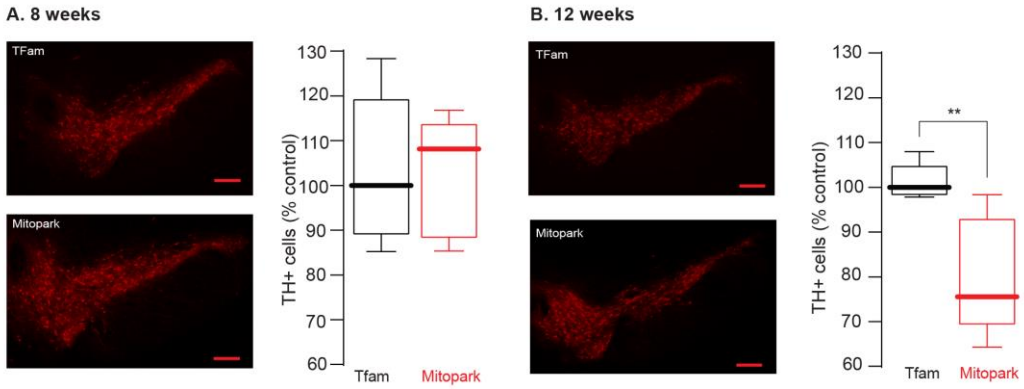

Figure 5. Substantia nigra pars compacta dopamine neurodegeneration. (A) Sample images (left) depicting tyrosine hydroxylase expressing (TH^+) neurons in SNc of Tfam amd mitopark mice; scale bars denote 200 µm; TH staining in red. Quantified data (right) indicate that at 8 weeks there is no change in the number of TH^+ cells in the SNc; Tfam n = 6 and mitopark n = 6 mice. (B) Sample images (left) depicting tyrosine hydroxylase expressing (TH^+) neurons in SNc of Tfam amd mitopark mice; scale bars denote 200 µm; TH staining in red. Quantified data (right) indicate that at 12 weeks there is significant loss in the number of TH^+ cells in the SNc; Tfam n = 6 and mitopark n = 6 mice. Data analyzed using Mann-Whitney test; $*p < 0.05$

3.2 Habit acquisition and early Parkinson's disease

Motor symptoms emerge in the mitopark mice at 12 weeks of age (Ekstrand et al., 2007; Li et al., 2013; Chen et al., 2019). Thus, the period before 12 weeks of age can be considered as the pre-motor phase. Previous studies indicate that at eight weeks of age, mitopark mice exhibit impaired novel object recognition, learning memory deficits in the Barnes maze, and spatial deficits in the Moris water maze (Li et al., 2013; Langley et al., 2021). The dorsolateral striatum regulates habitual responding, and previous studies indicate that lesions to the striatum or nigrostriatal pathway impair habit acquisition in rodents (Yin et al., 2004; Faure et al., 2005; Nadel et al., 2020). In mitopark mice, striatal DA deficits begin at eight weeks of age (Chen et al., 2019), and as indicated above, there is no SNc neurodegeneration at this point. Thus, we decided to evaluate if habit acquisition

is impaired in 8 week old mitopark mice during the pre-motor phase of PD. To assess habit learning, mice were trained to perform an instrumental action (pressing lever) to obtain a highly valued reward (sugar pellet). The instrumental action can transform from a goal-directed to a habitual response after extensive training and become progressively less sensitive to a devaluation of outcome (Dickinson et al., 1983). Thus, a decrease in sensitivity to devaluation can be measured as a behavioral readout of habit learning.

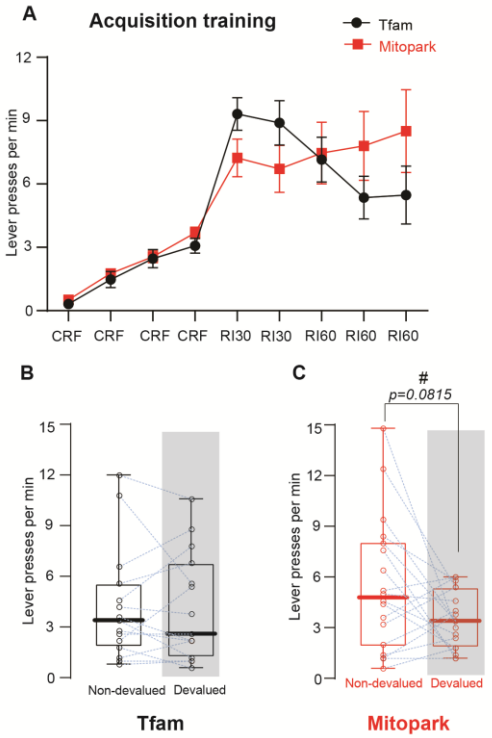

Figure 6. Impaired habit acquisition trend in early Parkinson's disease (A) Lever presses per minute during training phase. CRF, continuous reinforcement; RI30, random interval 30 s; RI60, random interval 60 s. A two-way mixed ANOVA conducted for acquisition training, with days and genotype as factors, showed no main effect of genotype ($F_{(1, 17)}$ = 0.09879, p=0.7571), a main effect of days ($F_{(8,136)}$ = 25.87, p< 0.0001), and an interaction between these factors ($F_{(8,91)}$= 2.17, p=0.037). All mice regardless of their genotype learned lever pressing task. (B) and (C) Outcome devaluation test for Tfam and mitopark mice respectively. Shaded region represents devalued condition. Devalued, mice received 1h of ad libitum exposure to unlimited sugar pellets, same as earned by lever pressing. Non-devalued, mice received 1h of ad libitum exposure to unlimited standard chow, which controls for the overall level of satiety. After the pre-exposure, all mice were given a 5 min probe test conducted in extinction. The comparison is within subjects: each mouse was given the devaluation and control treatments on consecutive days, controlled for order. Data was quantified using Mann-Whitney test. Upon devaluation Tfam mice sustained lever pressing action (p=0.877), where as mitopark mice showed reduced lever pressing action (p=0.0815). Tfam n = 15 and mitopark n = 18 mice

Both mitopark and control mice learned to press the lever on a training protocol consisting of 4 days of continuous reinforcement (CRF), 2 days of random interval (RI) 30 s, and 3 days of RI 60 s schedules (Yu et al., 2009). A two-way mixed ANOVA conducted for acquisition training (Fig 6A), with days and genotype as factors, showed no main effect of genotype ($F_{(1, 17)}$ = 0.09879, p=0.7571), a main effect of days ($F_{(8,136)}$ = 25.87, p< 0.0001), and an interaction between these factors ($F_{(8,91)}$= 2.17, p=0.037). All mice, regardless of the genotype, increased their lever pressing rate during acquisition training.

After acquisition training, a devaluation test was performed using a specific satiety procedure (Yu et al., 2009) wherein devalued mice received 1h of ad libitum exposure to unlimited sugar pellets, the same as earned by lever pressing. Non-devalued mice received1h of ad libitum exposure to unlimited standard chow, which controls for the overall level of satiety. After the pre-exposure, all mice were given a 5 min probe test conducted in extinction. Comparison of lever-pressing data from the devaluation test showed that the Tfam mice sustained the lever-pressing action (Fig. 6B); there was no difference between the devalued and non-devalued conditions (p=0.877). Thus, the behavior of Tfam mice was insensitive to reward devaluation, indicating the lever pressing was habitual. Mitopark mice similarly acquired the lever pressing task but showed reduced lever press during the probe test for the devalued condition with a p-value of 0.0815 (Fig. 6C). This suggests that mitopark mice failed to develop the lever-pressing habit despite extensive training, and their action may remain goal-directed.

3.3 Striatal changes in early Parkinson's disease

As indicated above, mitopark mice showed reduced lever pressing during the devaluation test, suggesting that habit formation might be impaired during the pre-motor phase of PD. The dorsolateral striatum (DLS) is the hub of habitual responding (Yin et al., 2004; Faure et al., 2005; Nadel et al., 2020). To investigate what happens to the DLS during this pre-motor phase, we decided to characterize dSPNs and iSPNs in DLS at eight weeks of age in Tfam and mitopark mice. eGFP expressing iSPNs and tdTomato expressing dSPNs were identified based on fluorescence expression, and whole-cell patch-clamp electrophysiology was performed to assess the intrinsic excitability. A two-way mixed ANOVA was used to analyze intrinsic excitability. There was no change in the number of action potentials generated by injecting depolarizing current in dSPNs (Fig. 7A). In contrast, in iSPNs injecting depolarizing current produced an increase in the number of action potentials in DLS brain slices of the mitopark mice (Fig. 7B); more specifically,

depolarizing current injection of 260-500pA produced significantly more action potentials in iSPNs from mitopark mice compared to Tfam mice. Despite showing increased intrinsic excitability, no other membrane properties were changed. Tables 2 and 3 summarizes the membrane properties of iSPNs and dSPNs at eight weeks of age, respectively.

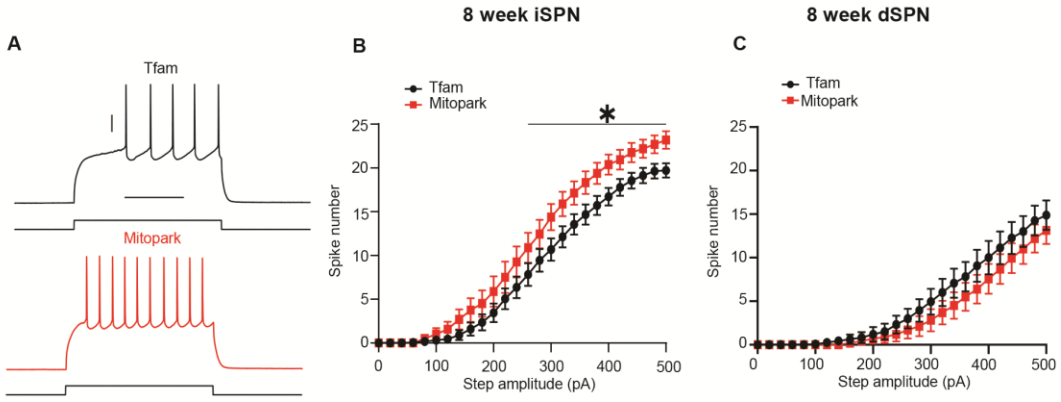

Figure 7. Indirect pathway spiny projection neuron intrinsic excitability was increased in early Parkinson's disease. (A) Sample traces for iSPNs at 260 pA illustrating changes in the inctrinsic excitability are provided with vertical and horizontal scale bars denoting 20mV and 200 ms, respectively and (B) Current–response curves for iSPNs in 8 week old mice show increased spike number for 260-500pA deploarizing currents (*p<0.05); Tfam n = 22 and mitopark n= 16 cells. A two-way mixed ANOVA conducted for iSPN intrinsic excitability, with current and genotype as factors, showed no main effect of genotype ($F_{(1, 21)}$ = 3.856, p= 0.0629), a main effect of current ($F_{(25, 525)}$ = 310.0, p< 0.0001), and an interaction between these factors ($F_{(25, 369)}$ = 2.169, p=0.0012). (C) Current–response curves for dSPNs in 8 week old mice show no change in intrinsic excitability; Tfam n = 16 and mitopark n= 16 cells. A two-way mixed ANOVA conducted for dSPN intrinsic excitability, with current and genotype as factors, showed no main effect of genotype ($F_{(1, 15)}$ = 1.104, p= 0.3101), a main effect of current ($F_{(25, 375)}$ = 67.53, p< 0.0001), and no interaction between these factors ($F_{(25, 375)}$ = 0.7834, p= 0.7639).

Table 2 : Membrane properties of iSPN at eight weeks of age

Membrane property	Tfam			Mitopark			p value
	25th quartile	Median	75th quartile	25th quartile	Median	75th quartile	
Rheobase	175	210	245	125	200	235	0.2167
Resting membrane potential (RMP)	-83.53	-80.59	-77.85	-82.71	-81.58	-80.39	0.9884
Threshold	-48.16	-42.62	-38.06	-48.73	-45.79	-40.32	0.2876
Action potential (AP) height	55.76	74.14	80.27	55.23	74.23	86.62	0.7814
Input resistance	0.6628	0.6834	0.7035	0.6725	0.6927	0.7179	0.609
Afterhyperpolarization (AHP) amplitude	9.216	12.31	14.18	8.308	9.262	12.89	0.151

Table 3 : Membrane properties of dSPN at eight weeks of age

Membrane property	Tfam			Mitopark			p value
	25th quartile	Median	75th quartile	25th quartile	Median	75th quartile	
Rheobase	225	300	385	270	320	410	0.364
Resting membrane potential (RMP)	-87.06	-85.26	-79.04	-85.39	-82.55	-79.52	0.3045
Threshold	-46.58	-41	-38.06	-42.6	-39.86	-36.44	0.2388
Action potential (AP) height	54.89	71.62	79.47	63.36	69.61	80.94	0.8965
Input resistance	0.6739	0.7059	0.736	0.6599	0.6815	0.709	0.0938
Afterhyperpolarization (AHP) amplitude	10.69	11.51	13.32	10.22	12.76	14.06	0.7449

As discussed previously, a hallmark of the parkinsonian striatum is spine pruning in SPNs. To examine whether this similarly occurred in a model of early PD, 2PLSM was utilized to examine spine density. Both proximal and distal shafts were evaluated for spine density. There was no spine pruning in both the SPNs during premotor PD (Fig. 8).

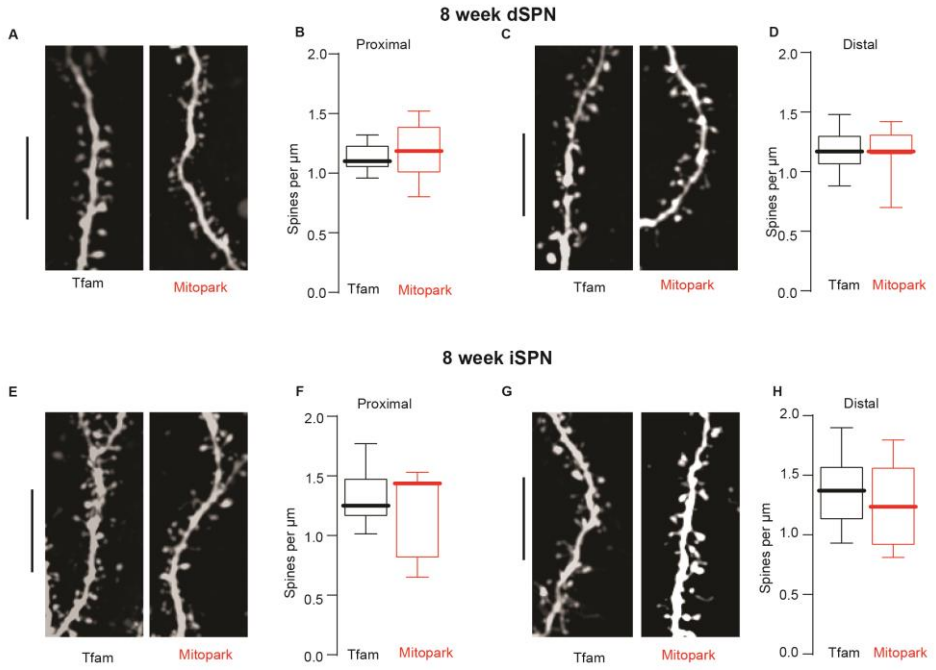

Figure 8. Spine density was unchanged in early Parkinson's disease. (A) & (C) representative 2PLSM images of proximal and distal dentrite of dSPN from Tfam (black) and mitopark (red) mice, vertical scale bar denotes 10 µm. There was no difference in dSPN proximal (B) and distal (D) spine density. For proximal dentrite , Tfam n = 19 and mitopark n = 15. For distal dentrite, Tfam n = 19 and mitopark n = 15. (E) & (G) representative 2PLSM images of proximal and distal dentrite of iSPN from Tfam (black) and mitopark (red) mice, vertical scale bar denotes 10 µm. There was no difference in iSPN proximal (F) and distal (H) spine density. For proximal dentrite, Tfam n = 24 and mitopark n = 16. For distal dentrite, Tfam n = 23 and mitopark n = 17.

3.4 Indirect spiny projection neuron changes associated with loss of TH$^+$ cells in substantia nigra pars compacta

Since iSPNs display increased excitability at eight weeks of age, we sought to determine if DLS iSPN dysfunction persisted or progressed at a time point when TH$^+$ cells are lost in the SNc. At 12 weeks of age, mice exhibit ~25% neuronal loss, which coincides with motor impairments (Ekstrand et al., 2007; Li et al., 2013; Chen et al., 2019). Again whole-cell patch-clamp recordings were performed on iSPNs in the DLS to assess intrinsic excitability with 2PLSM to examine spine density. A two-way mixed ANOVA indicated a significant increase in the intrinsic excitability of iSPNs, indicated by an increase in the number of action potential firing (Fig. 9).

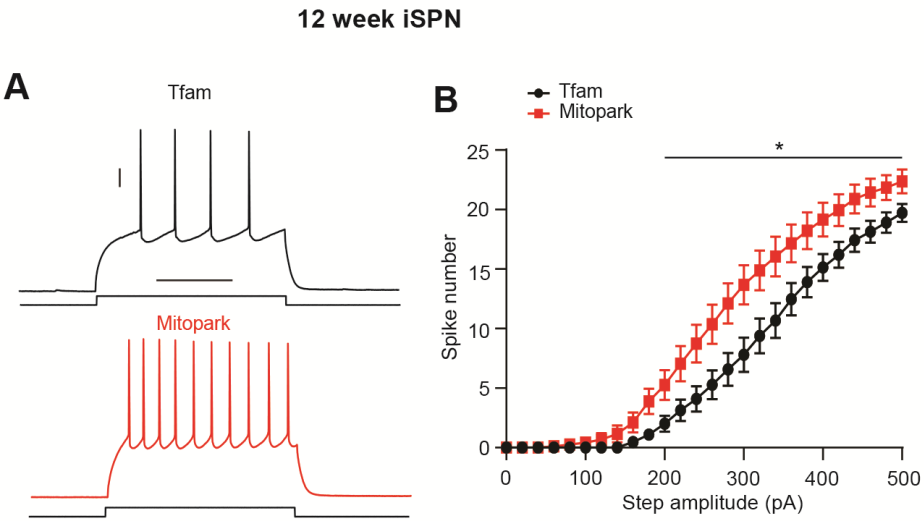

Figure 9. Indirect spiny projection neuron dysfuntion persists when TH+ cells are lost in substantia nigra pars compacta. (A) Sample traces at 200 pA illustrating changes in the inctrinsic excitability are provided with vertical and horizontal scale bars denoting 20mV and 200 ms, respectively and (B) Current–response curves for iSPNs in 12 week old mitopark mice show significant increase in spike number from 200-500pA (*p<0.05); Tfam n = 21 and mitopark n = 19 cells. A two-way mixed ANOVA conducted for iSPN intrinsic excitability, with current and genotype as factors, showed main effect of genotype ($F(1, 20) = 6.770$, $p=0.0171$), a main effect of current ($F(25, 500) = 248.1$, $p< 0.0001$), and interaction between these factors ($F(25, 448) = 4.100$, $p< 0.0001$).

Unlike the results from 8 week mice, the change in iSPN intrinsic excitability at 12 weeks of age was associated with changes in membrane properties (see table 4). There is a significant decrease in after-hyperpolarization amplitude ($p<0.05$) and a trend for a decrease in threshold and rheobase. In addition to the persistent and qualitatively more robust increased intrinsic excitability, spine pruning was also evident.

Table 4: Membrane properties of iSPNs at twelve weeks of age

Membrane property	Tfam			Mitopark			p-value
	25th quartile	Median	75th quartile	25th quartile	Median	75th quartile	
Rheobase	180	240	320	160	180	240	0.0771
Resting membrane potential (RMP)	-84.43	-82.85	-81.45	-84.99	-82.51	-80.93	0.7277
Threshold	-45.59	-40.44	-37.81	-49.35	-44.74	-39.98	0.0547
Action potential (AP) height	55.45	61.28	73.58	60.61	69.31	81.39	0.1253
Input resistance	0.6811	0.697	0.7073	0.6624	0.7065	0.7208	0.5919
Afterhyperpolarization (AHP) amplitude	10.39	12.33	13.96	8.575	10.77	11.47	0.019

At 12 weeks of age iSPN spine density was decreased in mitopark mice compared to age-matched tfam control subjects (Fig. 10). While the proximal shaft showed no spine pruning, there is a significant decrease in distal spine density ($p<0.05$), suggesting spine pruning may begin at the distal dendrites, and with disease progression, advance to proximal sites.

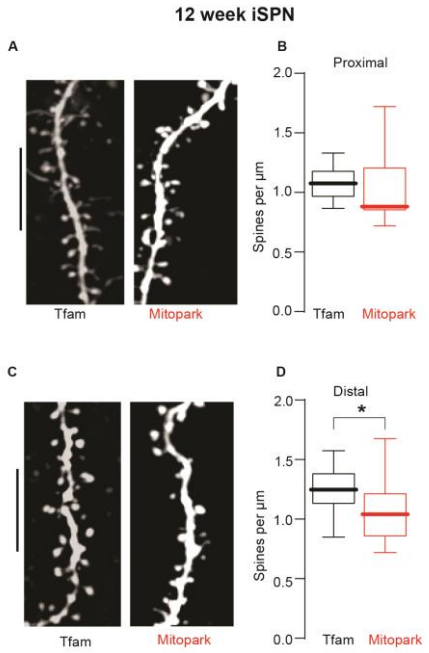

Figure 10. Decreased spine density in the distal dendrite of indirect spiny projection neuron after the loss of TH$^+$ cells in substantia nigra pars compacta (A) & (C) representative 2PLSM images of proximal and distal dentrite of iSPN from Tfam (black) and mitopark (red) mice, vertical scale bar denotes 10 µm. There is decrease in spine density for distal (D) but not the proximal (B) dendrite of iSPN. Data analyzed using Mann-Whitney test; *$p < 0.05$. For proximal dentrite , Tfam n = 21 and mitopark n = 16. For distal dentrite, Tfam n = 20 and mitopark n = 17.

Chapter IV: Discussion

Clinical diagnosis of PD relies heavily on the emergence of the cardinal motor symptoms such as resting tremor, postural instability, and bradykinesia (Jankovic, 2008). Unfortunately, these symptoms are not visible until >50% of the SNc DA neurons degenerate, and more than 80 percent of the striatum is depleted of DA (Godau et al., 2012). Current therapeutics aim to alleviate the motor symptoms by restoring the DA balance, which effectively treats PD-related motor deficits; however, these treatments fail to attenuate the progressive degeneration. Prior to the emergence of these debilitating motor symptoms are years, sometimes decades called the premotor phase, during which patients are undiagnosed. During this period, patients may begin to experience non-motor symptoms (Goldman and Postuma, 2014; Weintraub and Mamikonyan, 2019). Thus, the slow presentation of symptoms in PD presents a substantial temporal window to potentially target and arrest neurodegeneration in the early stages of Parkinson's disease. The main findings from our studies suggest that in the mitopark mice, a preclinical transgenic model of progressive PD, there is a trend for impaired habit acquisition during early PD, and increased iSPNs activity contributes to striatal dysfunction in PD.

First described in 2007 by Ekstrand et al., mitopark mice were engineered to lack the Tfam gene specifically in midbrain dopaminergic neurons. The Tfam gene is of nuclear origin but is essential for mitochondrial DNA parameters, such as transcription initiation, repair, and maintenance of copy number (Larsson et al., 1998). This genetic manipulation resulted in mitochondrial respiratory chain deficits causing progressive SNc neurodegeneration as seen in human PD. Mitopark mice faithfully recapitulate key parkinsonian features, including progressive, selective loss of SNc DA neurons over that of the ventral tegmental area (VTA), spontaneous vertical and horizontal locomotor deficits that improve with L-DOPA treatment, cognitive dysfunction preceding motor impairments, and decreased striatal DA (Ekstrand et al., 2007; Galter et al., 2010; Good et al., 2011; Branch et al., 2016). They also reproduce the sex difference and GI disturbances associated with PD (Chen et al., 2019; Ghaisas et al., 2019). Thus the mitopark mouse model serves as an invaluable tool to bridge the gap in knowledge during the premotor phase of PD.

Beginning around 12 weeks and ranging up to 45 weeks of age, the mitopark mice experience progressive degeneration of the nigrostriatal pathway (Ekstrand et al., 2007; Ricke et al., 2020). Consistent with these reports, our study indicates significant loss in

SNc DA neurons at 12 weeks of age. Locomotor deficits emerge at 12 weeks of age and exacerbate as the disease progresses (Ekstrand et al., 2007; Li et al., 2013; Chen et al., 2019; Langley et al., 2021). However, cognitive dysfunction precedes the onset of motor symptoms in the mitopark mouse model of PD. At eight weeks of age, mitopark mice exhibit impaired novel object recognition, learning memory deficits in the Barnes maze, and spatial deficits in the Moris water maze (Li et al., 2013; Langley et al., 2021). Findings from our study indicate that at eight weeks of age, during operant conditioning, mitopark mice acquire lever pressing tasks but show reduced lever press upon reward devaluation, indicating that their actions are goal-directed. Despite extensive training, they fail to demonstrate habitual performance. Thus, impaired habit acquisition might be a trend during early PD and serve as a behavioral biomarker for the presymptomatic diagnosis of PD.

The striatum is the major output nuclei of the SNc dopaminergic neurons and is known to regulate movement and reward-related behaviors. The dorsolateral striatum (DLS) is the hub of habitual responding (Yin et al., 2004; Faure et al., 2005; Nadel et al., 2020). DLS electrophysiological recording from our study indicates that in mitopark mice during the premotor phase, there is increased iSPN excitability with intact dSPN activity with no changes in the membrane properties. Also, there is no evidence of spine pruning at eight weeks of age. A reduction in striatal DA release has also been observed at eight weeks of age in mitopark mice using fast-scan cyclic voltammetry (Good et al., 2011; Chen et al., 2019). This decrease in the striatal DA release might be the reason for increased iSPN activity during the premotor phase. Previous studies indicate that both dSPNs and iSPNs are likely to be engaged in both the learning and the execution of a habit (Bariselli et al., 2019). It is thought that dSPN activation promotes action performance, whilst iSPN activation plays an action-specific inhibitory and/or permissive role (Kravitz et al., 2010; Sippy et al., 2015). Thus, impaired habitual performance in mitopark mice during the premotor phase might be a behavioral consequence of increased iSPN activity.

At 12 weeks of age, mitopark mice exhibit neuronal loss, which coincides with significant motor impairments (Ekstrand et al., 2007; Li et al., 2013; Chen et al., 2019). The electrophysiological recordings from our study indicate that DLS iSPN dysfunction persisted, and qualitatively it appears to have increased in the magnitude. These findings support the traditional belief that there is an imbalance between the direct and indirect pathways and that hyperactivation of iSPNs likely contributes to the cardinal motor

symptoms of PD (Albin et al., 1989). Membrane properties also begin to change at this time point. There is a significant decrease in afterhyperpolarization (AHP) amplitude and a trend for decreased threshold and rheobase. AHP amplitude is governed by Ca^{2+} activated potassium channels. Dysregulation of these channels might decrease AHP amplitude, eventually resulting in increased intrinsic excitability. Voltage-gated sodium channels (VGSCs) play an essential role in the initiation and propagation of action potentials in neurons. An increase in VGSCs might be responsible for decreased threshold and increased intrinsic excitability of iSPNs. Rheobase is the minimal electrical current that is necessary to elicit an action potential when current is injected into a cell, and a decrease in the rheobase is consistent with increased excitability. At 12 weeks of age, iSPN distal dendrite underwent spine pruning. Using the 6-OHDA model to generate a full lesion, both proximal and distal spines undergo pruning (Fieblinger et al., 2014a). Together these data suggest that spine pruning may initiate at distal processes and with disease progression advance to proximal sites as well.

While the mitopark model serves as a valuable tool to study progressive degeneration as seen in humans, it has certain limitations. One caveat of this model is that it relies on DAT expression within cells, making it DA-centric. Another limitation is that the mitopark mouse model fails to take into account the role of individual genes that are responsible for familial forms of PD. Tfam itself has not been directly linked to PD pathogenesis (Belin et al., 2007). Therefore, although knocking out Tfam can dependably model mitochondrial impairment in DA neurons, it remains unclear if it mimics a specific component of the mitochondrial deficits commonly observed in PD (Beckstead and Howell, 2021).

In conclusion, there is no perfect model to study PD, but the mitopark mouse model is one of a kind as it mimics major human PD features. More studies need to be carried out to validate the mouse model further. Our study is the first to look at striatal dysfunction in mitopark mice and describes the timeline for the electrophysiological changes in the striatum during the progressive neurodegeneration in the mitopark mouse. Major findings from our study indicate that striatal dysfunction is apparent during the premotor phase of PD, and iSPNs are exclusively affected in PD. Also, there might be a trend for impaired habit acquisition during the premotor phase of PD. Hence, it can serve as a potential behavioral biomarker for the early detection of PD.

Bibliography

Adler CH (2011) Premotor symptoms and early diagnosis of Parkinson's disease. Int J Neurosci 121:3–8.

Albin RL, Young AB, Penney JB (1989) The functional anatomy of basal ganglia disorders. Trends Neurosci 12:366–375.

Augustin SM, Chancey JH, Lovinger DM (2018) Dual Dopaminergic Regulation of Corticostriatal Plasticity by Cholinergic Interneurons and Indirect Pathway Medium Spiny Neurons. Cell Rep 24:2883–2893.

Baldereschi M, Di Carlo A, Rocca WA, Vanni P, Maggi S, Perissinotto E, Grigoletto F, Amaducci L, Inzitari D (2000) Parkinson's disease and parkinsonism in a longitudinal study: Two-fold higher incidence in men. Neurology 55:1358–1363.

Balestrino R, Schapira AH V (2019) Parkinson disease. Eur J Neurol 2020:27–42.

Bariselli S, Fobbs WC, Creed MC, Kravitz A V. (2019) A competitive model for striatal action selection. Brain Res 1713:70–79.

Beckstead MJ, Howell RD (2021) Progressive parkinsonism due to mitochondrial impairment: Lessons from the MitoPark mouse model. Exp Neurol 341.

Belin AC, Björk BF, Westerlund M, Galter D, Sydow O, Lind C, Pernold K, Rosvall L, Håkansson A, Winblad B, Nissbrandt H, Graff C, Olson L (2007) Association study of two genetic variants in mitochondrial transcription factor A (TFAM) in Alzheimer's and Parkinson's disease. Neurosci Lett 420:257–262 Available at: http://www.aldrecentrum.se/snack.

Beninger RJ (1983) The role of dopamine in locomotor activity and learning. Brain Res Rev 6:173–196.

Berg D, Borghammer P, Fereshtehnejad SM, Heinzel S, Horsager J, Schaeffer E, Postuma RB (2021) Prodromal Parkinson disease subtypes — key to understanding heterogeneity. Nat Rev Neurol 17:349–361.

Berry KP, Nedivi E (2017) Spine Dynamics: Are They All the Same? Neuron 96:43–55.

Björklund A, Dunnett SB (2007) Dopamine neuron systems in the brain: an update. Trends Neurosci 30:194–202.

Bourne J, Harris KM (2007) Do thin spines learn to be mushroom spines that remember? Curr Opin Neurobiol 17:381–386.

Branch SY, Chen C, Sharma R, Lechleiter XJD, Li S, Beckstead MJ (2016) Dopaminergic Neurons Exhibit an Age-Dependent Decline in Electrophysiological Parameters in the MitoPark Mouse Model of Parkinson ' s Disease. 36:4026–4037.

Chen YH, Wang V, Huang EYK, Chou YC, Kuo TT, Olson L, Hoffer BJ (2019) Delayed dopamine dysfunction and motor deficits in female Parkinson model mice. Int J Mol Sci 20.

D'ardenne K, Eshel N, Luka J, Lenartowicz A, Nystrom LE, Cohen JD (2012) Role of prefrontal cortex and the midbrain dopamine system in working memory updating. Available at: www.pnas.org/cgi/doi/10.1073/pnas.1116727109.

Da Cunha C, Silva MHC, Wietzikoski S, Wietzikoski EC, Ferro MM, Kouzmine I, Canteras NS (2006) Place learning strategy of substantia nigra pars compacta-lesioned rats. Behav Neurosci 120:1279–1284.

Day M, Wang Z, Ding J, An X, Ingham CA, Shering AF, Wokosin D, Ilijic E, Sun Z, Sampson AR, Mugnaini E, Deutch AY, Sesack SR, Arbuthnott GW, Surmeier J (2006) Selective elimination of glutamatergic synapses on striatopallidal neurons in Parkinson disease models. Available at: http://www.nature.com/natureneuroscience.

Decamp E, Schneider JS (2004) Attention and executive function deficits in chronic low-dose MPTP-treated non-human primates. Eur J Neurosci 20:1371–1378.

Dickinson A, Nicholas DJ, Adams CD (1983) The effect of the instrumental training contingency on susceptibility to reinforcer devaluation. Q J Exp Psychol Sect B 35:35–51.

Du Y, Graves SM (2019) Spiny projection neuron dynamics in toxin and transgenic models of parkinson's disease. Front Neural Circuits 13:1–7.

Duda J, Pötschke C, Liss B (2016) Converging roles of ion channels, calcium, metabolic stress, and activity pattern of Substantia nigra dopaminergic neurons in health and Parkinson's disease. J Neurochem 139:156–178.

Duty S, Jenner P (2011) Animal models of Parkinson's disease: A source of novel treatments and clues to the cause of the disease. Br J Pharmacol 164:1357–1391.

Ekstrand MI, Gen Terzioglu M, Galter D, Zhu S, Hofstetter C, Lindqvist E, Thams S, Bergstrand A, Hansson S, Trifunovic A, Hoffer B, Cullheim S, Mohammed AH, Olson L, Larsson N-GR (2007) Progressive parkinsonism in mice with respiratory-chain-deficient dopamine neurons. Available at: www.pnas.orgcgidoi10.1073pnas.0605208103.

Escande M V., Taravini IRE, Zold CL, Belforte JE, Murer MG (2016) Loss of homeostasis in the direct pathway in a mouse model of asymptomatic parkinson's disease. J Neurosci 36:5686–5698.

Faure A, Haberland U, Condé F, El Massioui N (2005) Lesion to the nigrostriatal dopamine system disrupts stimulus-response habit formation. J Neurosci 25:2771–2780.

Fearnley JM, Lees AJ (1991) AGEING AND PARKINSON'S DISEASE: SUBSTANTIA NIGRA REGIONAL SELECTIVITY. Available at: https://academic.oup.com/brain/article/114/5/2283/399854.

Fieblinger T, Graves SM, Sebel LE, Alcacer C, Plotkin JL, Gertler TS, Chan CS, Heiman M, Greengard P, Cenci MA, Surmeier & DJ (2014a) ARTICLE Cell type-specific plasticity of striatal projection neurons in parkinsonism and L-DOPA-induced dyskinesia. Available at: www.nature.com/naturecommunications.

Fieblinger T, Graves SM, Sebel LE, Alcacer C, Plotkin JL, Gertler TS, Chan CS, Heiman M, Greengard P, Cenci MA, Surmeier DJ (2014b) Cell type-specific plasticity of striatal projection neurons in parkinsonism and L-DOPA-induced dyskinesia. Nat Commun 5.

Galter D, Pernold K, Yoshitake T, Lindqvist E, Hoffer B, Kehr J, Larsson NG, Olson L

(2010) MitoPark mice mirror the slow progression of key symptoms and L-DOPA response in Parkinson's disease. Genes, Brain Behav 9:173–181.

Gerfen CR (1988) Synaptic Organization of the Striatum.

Gerfen CR, Surmeier DJ (2011) Modulation of striatal projection systems by dopamine. Annu Rev Neurosci.

Ghaisas S, Langley MR, Palanisamy BN, Dutta S, Narayanaswamy K, Plummer PJ, Sarkar S, Ay M, Jin H, Anantharam V, Kanthasamy A, Kanthasamy AG (2019) MitoPark Transgenic Mouse Model Recapitulates the Gastrointestinal Dysfunction and Gut-Microbiome Changes of Parkinson's Disease HHS Public Access. Neurotoxicology 75:186–199.

Godau J, Hussl A, Lolekha P, Stoessl AJ, Seppi K (2012) Neuroimaging: Current role in detecting pre-motor Parkinson's disease. Mov Disord 27:634–643.

Goldman JG et al. (2018) Cognitive impairment in Parkinson's disease: a report from a multidisciplinary symposium on unmet needs and future directions to maintain cognitive health. 4:19 Available at: www.nature.com/npjparkd.

Goldman JG, Postuma R (2014) Premotor and non-motor features of Parkinson's disease. Curr Opin Neurobiol.

Gomez G, Escande M V, Suarez LM, Rela L, Belforte JE, Moratalla & R, Murer MG, Gershanik OS, Taravini IRE (2019) Changes in Dendritic Spine Density and Inhibitory Perisomatic Connectivity onto Medium Spiny Neurons in L-Dopa-Induced Dyskinesia. Available at: https://doi.org/10.1007/s12035-019-1515-4.

Good CH, Hoffman AF, Hoffer BJ, Chefer VI, Shippenberg TS, Bäckman CM, Larsson N, Olson L, Gellhaar S, Galter D, Lupica CR (2011) Impaired nigrostriatal function precedes behavioral deficits in a genetic mitochondrial model of Parkinson's disease. FASEB J 25:1333–1344.

Graves SM, Surmeier DJ (2019) Delayed spine pruning of direct pathway spiny projection neurons in a mouse model of parkinson's disease. Front Cell Neurosci 13:1–6.

Gülsüm Deniz Ö, Altun G, Kaplan A, Kübra Yurt K, Von Bartheld CS, Kaplan S (2018) A concise review of optical, physical and isotropic fractionator techniques in neuroscience studies, including recent developments. Available at: https://doi.org/10.1016/j.jneumeth.2018.07.012.

Gundersen HJG, Jensen EB V, Kieˆu K, Kieˆu K, Nielsen J (1999) The efficiency of systematic sampling in stereology-reconsidered.

Harris,' KM, Jensen,' FE, Tsao' B (1992) Three-Dimensional Structure of Dendritic Spines and Synapses in Rat Hippocampus (CAI) at Postnatal Day 15 and Adult Ages: Implications for the Maturation of Synaptic Physiology and Long-term Potentiation.

Hegarty S V, Nolan Y, Stoker TB, Torsney KM, Barker RA (2018) Emerging Treatment Approaches for Parkinson's Disease. Available at: www.frontiersin.org.

Jankovic J (2008) Parkinson's disease: clinical features and diagnosis. Available at: http://jnnp.bmj.com/.

Kin K, Yasuhara T, Kameda M, Date I (2019) Animal models for Parkinson's disease research: Trends in the 2000s. Int J Mol Sci 20.

Kitada T, Tong Y, Gautier CA, Shen J (2009) Absence of nigral degeneration in aged parkin/DJ-1/PINK1 triple knockout mice. J Neurochem 111:696–702.

Kravitz A V, Freeze BS, Parker PRL, Kay K, Thwin MT, Deisseroth K, Kreitzer AC (2010) LETTERS Regulation of parkinsonian motor behaviours by optogenetic control of basal ganglia circuitry. Nature.

Langley MR, Ghaisas S, Palanisamy BN, Ay M, Jin H, Anantharam V, Kanthasamy A, Kanthasamy AG (2021) Characterization of nonmotor behavioral impairments and their neurochemical mechanisms in the MitoPark mouse model of progressive neurodegeneration in Parkinson's disease. Exp Neurol 341.

Larsson N-G, Wang J, Wilhelmsson H, Oldfors A, Rustin P, Lewandoski M, Barsh GS, Clayton DA (1998) Mitochondrial transcription factor A is necessary for mtDNA maintenance and embryogenesis in mice. Available at: http://www.nature.com/naturegenetics.

Le W, Sayana P, Jankovic J (2014) Animal Models of Parkinson's Disease: A Gateway to Therapeutics? Neurotherapeutics.

Li X, Redus L, Chen C, Martinez PA, Strong R, Li S, O'connor JC (2013) South Texas Veterans Health Care System. Available at: www.plosone.org.

Lin KJ, Lin KL, Chen S Der, Liou CW, Chuang YC, Lin HY, Lin TK (2019) The overcrowded crossroads: Mitochondria, alpha-synuclein, and the endo-lysosomal system interaction in Parkinson's disease. Int J Mol Sci 20:1–28.

Maddox WT, Delis DC, Filoteo JV, Salmon DP (1996) Visual selective attention deficits in patients with Parkinson's disease: A quantitative model-based approach. Neuropsychology 10:197–218.

Magen I, Fleming SM, Zhu C, Garcia EC, Cardiff KM, Dinh D, De K, Rosa L, Sanchez M, Torres ER, Masliah E, David Jentsch J, Chesselet M-F (2012) Cognitive deficits in a mouse model of pre-manifest Parkinson's disease.

McNeill TH, Brown SA, Rafols JA, Shoulson I (1988) Atrophy of medium spiny I striatal dendrites in advanced Parkinson's disease. Brain Res 455:148–152.

Meiser J, Weindl D, Hiller K (2013) Complexity of dopamine metabolism. Cell Commun Signal 11:1–18.

Nadel JA, Pawelko SS, Copes-Finke D, Neidhart M, Howard CD (2020) Lesion of striatal patches disrupts habitual behaviors and increases behavioral variability. PLoS One 15:1–23.

Pchitskaya E, Bezprozvanny I (2020) Dendritic Spines Shape Analysis—Classification or Clusterization? Perspective. Front Synaptic Neurosci 12.

Pignatelli M, Bonci A (2015) Role of Dopamine Neurons in Reward and Aversion: A Synaptic Plasticity Perspective. Neuron 86:1145–1157.

Ricke KM, Paß T, Kimoloi S, Fährmann K, Jüngst C, Schauss A, Baris OR, Aradjanski M, Trifunovic A, Eriksson Faelker TM, Bergami M, Wiesner XRJ (2020)

Mitochondrial dysfunction combined with high calcium load leads to impaired antioxidant defense underlying the selective loss of nigral dopaminergic neurons. J Neurosci 40:1975–1986.

Sarkar S, Raymick J, Imam S (2016) Neuroprotective and therapeutic strategies against Parkinson's disease: Recent perspectives. Int J Mol Sci 17.

Schneider JS (1990) Chronic exposure to low doses of MPTP. II. Neurochemical and pathological consequences in cognitively-impaired, motor asymptomatic monkeys. Brain Res 534:25–36.

Shan Q, Ge M, Christie MJ, Balleine BW (2014) The acquisition of goal-directed actions generates opposing plasticity in direct and indirect pathways in dorsomedial striatum. J Neurosci 34:9196–9201.

Shen W, Flajolet M, Greengard P, Surmeier DJ (2008) Dichotomous dopaminergic control of striatal synaptic plasticity. Science (80-) 321:848–851.

Sippy T, Lapray D, Crochet S, Petersen CCH (2015) Cell-Type-Specific Sensorimotor Processing in Striatal Projection Neurons during Goal-Directed Behavior. Neuron 88:298–305.

Smolders S, Van Broeckhoven C (2020) Genetic perspective on the synergistic connection between vesicular transport, lysosomal and mitochondrial pathways associated with Parkinson's disease pathogenesis. Acta Neuropathol Commun 8:1–28.

Solari N, Bonito-Oliva A, Fisone G, Brambilla R (2013) Understanding cognitive deficits in Parkinson's disease: Lessons from preclinical animal models. Learn Mem 20:592–600.

Stoker TB, Greenland JC (2018) Preface.

Surmeier DJ, Ding J, Day M, Wang Z, Shen W (2007) D1 and D2 dopamine-receptor modulation of striatal glutamatergic signaling in striatal medium spiny neurons. Trends Neurosci 30:228–235.

Surmeier DJ, Graves SM, Shen W (2014) Dopaminergic modulation of striatal networks in health and Parkinson's disease. Curr Opin Neurobiol 29:109–117.

Thiele SL, Chen B, Lo C, Gertler TS, Warre R, Surmeier JD, Brotchie JM, Nash JE (2014) Selective loss of bi-directional synaptic plasticity in the direct and indirect striatal output pathways accompanies generation of parkinsonism and L-DOPA induced dyskinesia in mouse models. Available at: http://dx.doi.org/10.1016/j.nbd.2014.08.006.

Villalba RM, Smith Y (2018) Loss and remodeling of striatal dendritic spines in Parkinson's disease: from homeostasis to maladaptive plasticity? J Neural Transm 125:431–447.

Wager MGT and JFS (2011) 基因的改变NIH Public Access. Bone 23:1–7 Available at: https://www.ncbi.nlm.nih.gov/pmc/articles/PMC3624763/pdf/nihms412728.pdf.

Weintraub D, Mamikonyan E (2019) The Neuropsychiatry of Parkinson Disease: A Perfect Storm. Am J Geriatr Psychiatry 27:998–1018.

William Langston J, Ballard P, Tetrud JW, Irwin I (1983) Chronic parkinsonism in humans due to a product of meperidine-analog synthesis. Science (80-) 219:979–980.

Wright MJ, Burns RJ, Geffen GM GL (1990) COVERT ORIENTATION OF VISUAL ATTENTION IN PARKINSON'S DISEASE: AN IMPAIRMENT IN THE MAINTENANCE OF ATTENTION. Neuropsychologia.

Xie W, Li X, Li C, Zhu W, Jankovic J, Le W (2010) Proteasome inhibition modeling nigral neuron degeneration in Parkinson's disease. J Neurochem 115:188–199.

Yin HH, Knowlton BJ, Balleine BW (2004) Lesions of dorsolateral striatum preserve outcome expectancy but disrupt habit formation in instrumental learning. Eur J Neurosci 19:181–189.

Yu C, Gupta J, Chen JF, Yin HH (2009) Genetic deletion of A2A adenosine receptors in the striatum selectively impairs habit formation. J Neurosci 29:15100–15103.

Zhang S, Wang R, Wang G (2019) Impact of Dopamine Oxidation on Dopaminergic Neurodegeneration. ACS Chem Neurosci.

Ztaou S, Lhost J, Watabe I, Torromino G, Amalric M (2018) Striatal cholinergic interneurons regulate cognitive and affective dysfunction in partially dopamine-depleted mice. Eur J Neurosci 48:2988–3004.